THE JOURNAL OF BIOLOGICAL CHEMISTRY VOL. 292, NO. 6, pp. 2217–2225, February 10, 2017


# Deciphering Key Residues Involved in the Virulence-promoting Interactions between *Streptococcus pneumoniae* and Human Plasminogen*[S]

Received for publication, October 27, 2016, and in revised form, December 23, 2016 Published, JBC Papers in Press, December 23, 2016, DOI 10.1074/jbc.M116.764209

**Christophe Moreau**[1,2], **Rémi Terrasse**[1,3], **Nicole M. Thielens, Thierry Vernet, Christine Gaboriaud**[4], **and Anne Marie Di Guilmi**[5]

*From the Institut de Biologie Structurale (IBS), Université Grenoble Alpes, Commissariat à l'Energie Atomique (CEA), CNRS, 38044 Grenoble, France*

**Edited by Norma Allewell**

**Bacterial pathogens recruit circulating proteins to their own surfaces, co-opting the host protein functions as a mechanism of virulence. Particular attention has focused on the binding of plasminogen (Plg) to bacterial surfaces, as it has been shown that this interaction contributes to bacterial adhesion to host cells, invasion of host tissues, and evasion of the immune system. Several bacterial proteins are known to serve as receptors for Plg including glyceraldehyde-3-phosphate dehydrogenase (GAPDH), a cytoplasmic enzyme that appears on the cell surface in this moonlighting role. Although Plg typically binds to these receptors via several lysine-binding domains, the specific interactions that occur have not been documented in all cases. However, identification of the relevant residues could help define strategies for mitigating the virulence of important human pathogens, such as *Streptococcus pneumoniae* (Sp). To shed light on this question, we have described a combination of peptide-spot array screening, competition and SPR assays, high-resolution crystallography, and mutational analyses to characterize the interaction between SpGAPDH and Plg. We identified three SpGAPDH lysine residues that were instrumental in defining the kinetic and thermodynamic parameters of the interaction. Altogether, the integration of the data presented in this work allows us to propose a structural model for the molecular interaction of the SpGAPDH-Plg complex.**

Both bacterial commensalism and infectious process result from a complex interplay between the microbial agent and the host organism. The plasminogen/plasmin (Plg/Plm)[6] system is pivotal in the long-term relationship between bacteria and host. The recruitment of host Plg to the bacterial surface is a virulence strategy used by many pathogens that contributes to adhesion to host cell receptors and/or to extracellular macromolecules, to invasion of host tissues, and to evasion from the immune system (1).

The zymogen Plg is secreted by liver cells, circulates in the bloodstream, and is present in extracellular body fluids. Plg is converted into active Plm by proteolytic cleavage mediated by host-expressed tissue-type Plg activator and urokinase (2). The Plm is composed by the active protease domain linked by two disulfide bonds to the heavy chain composed of five homologous Kringle domains (K1–5), which contain lysine-binding sites.

Although the main physiological function of Plm is to degrade the fibrin network, Plm displays a broad-substrate spectrum including non-collagenous extracellular matrix proteins such as fibrinogen, fibrin, laminin, and fibronectin, facilitating cell migration in tissues. In addition, Plm activates matrix metalloproteases and elastase, which regulate wound healing, tissue remodeling, tumor metastasis, and angiogenesis (3, 4). Different strategies have been elaborated by bacteria to hijack the host Plg/Plm system: Plg/Plm associate directly either to bacterial proteins exposed at the cell surface or to fibrinogen, which decorates the bacterial surface through receptor-specific interaction. Consequently, the Plm bound to bacterial cells allows bacteria to degrade a vast range of host proteins promoting bacterial pathogenesis.

*Streptococcus pneumoniae* (the pneumococcus) is a member of the commensal flora of the upper respiratory tract in humans but also displays a high virulence potential. The pneumococcus is a leading cause of otitis, rhinitis, and sinusitis and of invasive life-threatening infections such as pneumonia, septicemia, and meningitis, resulting from the dissemination of pneumococci into the lungs, the bloodstream, and from the crossing over of the blood-brain barrier (5). Recruitment of Plg by pneumococcal cells has been shown to facilitate bacterial adherence to epithelial and endothelial cells, whereas internalization was not

* This work was supported by a Ph.D. grant from the Grenoble Alpes University (to C. M.). This work was also supported by a Ph. D. grant from the Rhône-Alpes region, Cluster Infectiologie (to R. T.). The authors declare that they have no conflicts of interest with the contents of this article.
[S] This article contains supplemental Table S2 and Fig. S1.
*The atomic coordinates and structure factors (code 5M6D) have been deposited in the Protein Data Bank (http://wwpdb.org/).*
[1] Both authors contributed equally to this work.
[2] Present address: Structural Genomic Consortium, University of Oxford, Headington, Oxford OX3 7DQ United Kingdom.
[3] Present address: Jacobs-University Bremen, 28759 Bremen, Germany.
[4] To whom correspondence may be addressed. Tel.: 33-4-57-42-85-99; E-mail: christine.gaboriaud@ibs.fr.
[5] To whom correspondence may be addressed. Tel.: 33-4-57-42-86-34; E-mail: anne-marie.di-guilmi@ibs.fr.
[6] The abbreviations used are: Plg, plasminogen; Plm, plasmin; Sp, *Streptococcus pneumoniae*; CBP, choline-binding protein; ACA, 6-aminocaproic acid; Pce, phosphorylcholine esterase; HsaGAPDH, *Homo sapiens* GAPDH; SauGAPDH, *Staphylococcus aureus* GAPDH; PGK, phosphoglycerate kinase; RU, response units; HBS, HEPES-buffered saline.

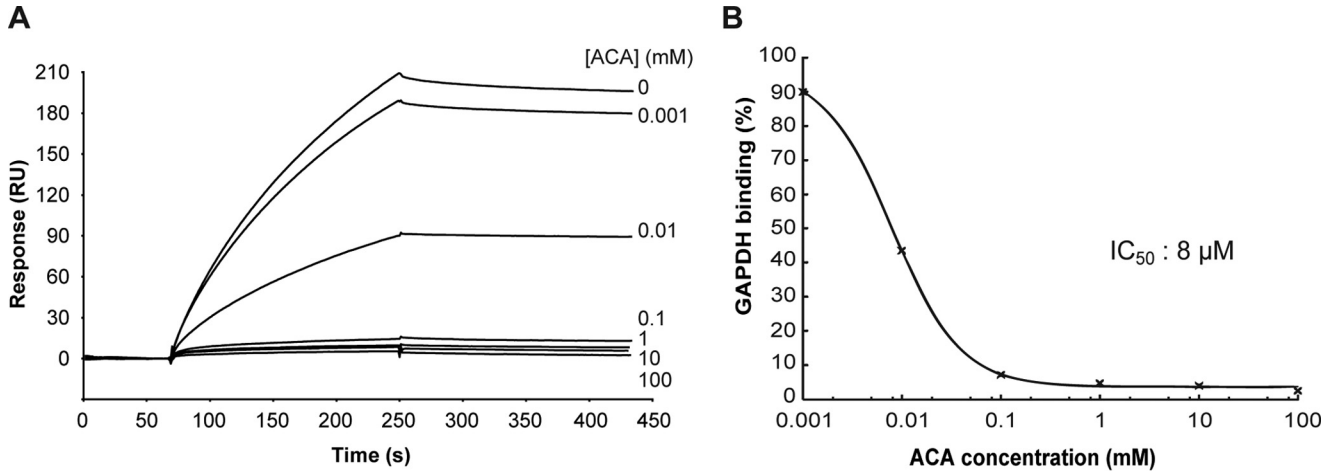


FIGURE 1. **SPR analysis of the competition of 6-aminocaproic acid for SpGAPDH binding to immobilized Plg.** *A*, SpGAPDH (100 nM) was injected over immobilized Plg (2625 RU) at 30 $\mu$l/min in HBS-CaP in the presence of the indicated concentrations of ACA. *B*, the specific signal obtained at the end of a 90-$\mu$l injection in the presence of ACA was compared with the value measured in its absence (considered as 100%). The $IC_{50}$ value was calculated from the plots of bound SpGAPDH *versus* ACA concentration (log scale). These results are representative of two independent experiments.

affected (6). In a previous work, we observed that coating of *S. pneumoniae* with Plg increased adherence to epithelial and endothelial cells *in vitro*, whereas Plm-coated pneumococci induced disruptions of monolayer cell junctions through cleavage of cadherin, the main component of adherens junctions. These data indicate that Plg recruitment might promote migration of pneumococci through cell barriers by a pericellular route (7).

Pneumococcal Plg receptors include proteins attached to the polysaccharide components of the cell wall: choline-binding proteins (CBPs) and peptidoglycan-linked proteins (8–11) as well as cytoplasmic enzymes that exert additional biological functions ("moonlighting") at the cell surface (12–14) such as enolase and glyceraldehyde-3-phosphate dehydrogenase (GAPDH) (15–17). In this study, we identify key SpGAPDH lysine residues involved in the interaction with Plg using a combination of peptide-spot array screening, competition and SPR assays, high-resolution structure of SpGAPDH, and mutational analyses. Hijacking the Plg system by eukaryotic and prokaryotic pathogens is an important issue in the outcome of infectious diseases. Most of the Plg ligands at the surface of pathogens are moonlighting proteins, among which GAPDH is one of the most represented. This work focuses on the complete characterization of the interaction between SpGAPDH and human Plg. The structural and functional data obtained identify the SpGAPDH residues involved in the interaction, and the bioinformatics analysis shows how these residues are conserved in a wide range of bacterial GAPDH, which suggests a more general interaction model.

## Results

*Lysine Residues of SpGAPDH Are Involved in Plg Recognition*—The Kringle domains of Plg contain lysine-binding sites formed by a charged and hydrophobic cleft that mostly bind C-terminal and internal lysine residues. The possible involvement of lysine residues in the interaction between SpGAPDH and Plg was thus investigated by SPR spectroscopy (Fig. 1*A*). Stable interaction of soluble SpGAPDH (100 nM) to immobilized Plg was observed, and inhibition was tested by the addition of 6-aminocaproic acid (ACA), a lysine analog. Complete inhibition was observed at about 100 $\mu$M ACA (Fig. 1*B*). The inhibition experiment was performed twice, and very close $IC_{50}$ values were obtained (8–10 $\mu$M) (Fig. 1*B*). These data strongly suggest that lysine residues contribute to SpGAPDH-Plg interaction.

*Mapping SpGAPDH Peptides Involved in Plg Recognition*—A peptide mapping procedure was used to identify lysine residues committed to the association of SpGAPDH with Plg. The SpGAPDH sequence was divided into 33 peptides (p1 to p33, Table 1). Each peptide was 20 amino acids long and overlapped the previous peptide by 10 amino acids. Peptides were fixed to the nitrocellulose membrane together with BSA and SpGAPDH used as negative and positive controls, respectively. The membrane was incubated with Plg, and bound Plg was detected with an anti-Plg antibody. Quantification of the chemiluminescence signal was performed, and the data obtained in four independent experiments are shown (Fig. 2). The signal detected with SpGAPDH was normalized to 100%. Peptide binding was considered significant when the values in at least two independent experiments were (i) 30% greater than the one observed with SpGAPDH and (ii) at least five times the one of BSA (with the exception of the data set shown in *dark gray*, which displayed a high background). Using these cut-off values, eight peptides were retained: p2, p12, p15, p16, p18, p29, p30, and p31. Of note, peptides p12 and p31 display the most important signal (up to 200% the SpGAPDH value) in three of the four experiments (Fig. 2). Although contiguous SpGAPDH peptides contain redundant sequence, they might not display comparable binding properties with Plg. Neither p11 nor p13 was detected, whereas p12 revealed a high score. The same is true for p18. On the contrary, p29, p30, and p31 peptides show significant binding to Plg, suggesting that the common sequence of these peptides might contain part of the SpGAPDH-binding site for Plg (Table 1).

*Competitive Inhibition of Plg Binding to SpGAPDH by Synthetic Peptides*—To further characterize the Plg-binding site of SpGAPDH, a competition assay was performed to test the

**TABLE 1**
**Peptides used in this study**
Residues in boldface were targeted for site-directed mutagenesis.

| Peptide | Sequence | Amino acids |
|---|---|---|
| p1 | VKVGI NGFGR IGRLA FRRIQ | 3–22 |
| p2 | IGRLA FRRIQ NVEGV EVTRI | 13–32 |
| p3 | NVEGV EVTRI NDLTD PVMLA | 23–42 |
| p4 | NDLTD PVMLA HLLKY DTTQG | 33–52 |
| p5 | HLLKY DTTQG RFDGT VEVKE | 43–62 |
| p6 | RFDGT VEVKE GGFEV NGKFI | 53–72 |
| p7 | GGFEV NGKFI KVSAE RDPEQ | 63–82 |
| p8 | KVSAE RDPEQ IDWAT DGVEI | 73–92 |
| p9 | IDWAT DGVEI VLEAT GFFAK | 83–102 |
| p10 | VLEAT GFFAK KEAAE KHLKG | 93–112 |
| p11 | KEAAE KHLKG GAKKV VITAP | 103–122 |
| p12 | GAKKV VITAP GGNDV KTVVF | 113–132 |
| p13 | GGNDV KTVVF NTNHD VLDGT | 123–142 |
| p14 | NTNHD VLDGT ETVIS GASCT | 133–152 |
| p15 | ETVIS GASCT TNCLA PMAKA | 143–162 |
| p16 | TNCLA PMAKA LQDNF GVVEG | 153–172 |
| p17 | LQDNF GVVEG LMTTI HAYTG | 163–182 |
| p18 | LMTTI HAYTG DQMIL DGPHR | 173–192 |
| p19 | DQMIL DGPHR GGDLR RARAG | 183–202 |
| p20 | GGDLR RARAG AANIV PNSTG | 193–212 |
| p21 | AANIV PNSTG AAKAI GLVIP | 203–222 |
| p22 | AAKAI GLVIP ELNGK LDGSA | 213–232 |
| p23 | ELNGK LDGSA QRVPT PTGSV | 223–242 |
| p24 | QRVPT PTGSV TELVA VLEKN | 233–252 |
| p25 | TELVA VLEKN VTVDE VNAAM | 243–262 |
| p26 | VTVDE VNAAM KAASN ESYGY | 253–272 |
| p27 | KAASN ESYGY TEDPI VSSDI | 263–282 |
| p28 | TEDPI VSSDI VGMSY GSLFD | 273–292 |
| p29 | VGMSY GSLFD ATQTK VLDVD | 283–302 |
| p30 | ATQTK VLDVD GKQLV KVVSW | 293–312 |
| p31 | GKQLV KVVSW YDNEM SYTAQ | 303–322 |
| p32 | YDNEM SYTAQ LVRTL EYFAK | 313–332 |
| p33 | LVRTL EYFAK IAK | 323–335 |

inhibitory property of the SpGAPDH-derived synthetic peptides. Plg was coated on a 96-well plate and incubated with positive peptides used at different concentrations, from 0.1 to 100 $\mu$g/ml, and subsequent binding of SpGAPDH was measured (Fig. 3). Seven of the eight peptides interacting with Plg were tested as well as p33, which contains the C-terminal lysine residue proposed to be involved in Plg interaction (18). No interaction with Plg was observed with p33 in peptide screening and competition assays, indicating that the C-terminal lysine residue most probably does not play a major role in Plg binding. No inhibition of the interaction between SpGAPDH and Plg was observed with p15, suggesting that the result from the dot-blot assay might be considered as a false positive (the same is true for p16, although this peptide was not included in the competition test). Association of SpGAPDH with Plg was significantly inhibited by peptides p12 and p31 in a dose-dependent manner. For the highest peptide concentration of 100 $\mu$g/ml, the level of inhibition was 36 and 72% for p12 and p31, respectively. This result is consistent with the observation that both peptides displayed the strongest interaction with Plg when assayed by the dot-blot assay (Fig. 2). In conclusion, two regions in SpGAPDH have been identified as part of the Plg-binding site: $^{113}$GAKKVVITAPGGNDVKTVVF$^{132}$ (p12) and $^{303}$GKQLVKVVSWYDNEMSYTAQ$^{322}$ (p31).

*Crystal Structure of SpGAPDH*—The X-ray structure of SpGAPDH has been solved and refined to 2.0 Å, with one dimer per asymmetric unit (Table 2) (Protein Data Bank (PDB): 5M6D). There is one SpGAPDH tetramer per unit cell because

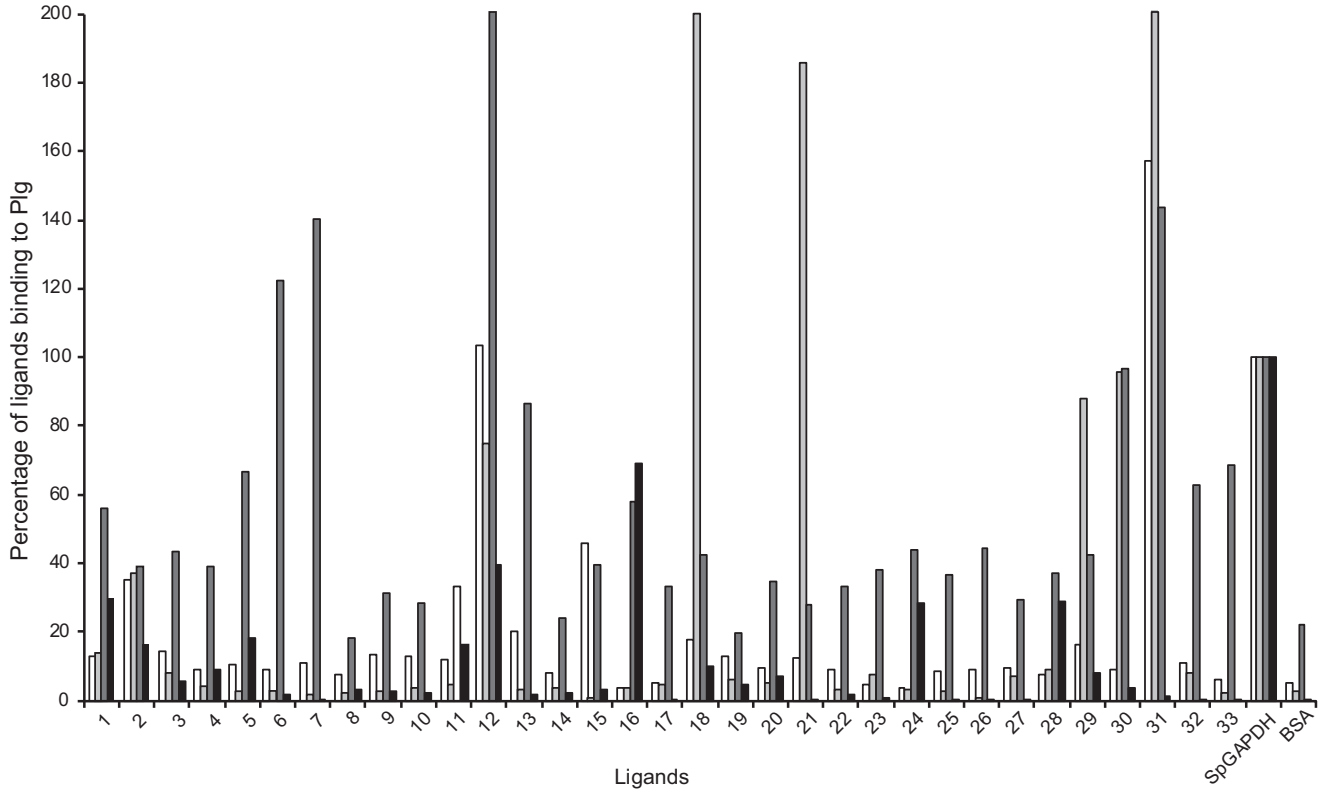


FIGURE 2. **Binding of Plg to SpGAPDH peptides.** Peptides were resuspended in water, and 10 $\mu$g of each peptide were spotted on a nitrocellulose membrane. Purified SpGAPDH and BSA proteins (10 $\mu$g) were also spotted and then selected as positive and negative controls, respectively. The membrane was incubated with Plg at 10 $\mu$g/ml and revealed with an anti-Plg antibody. SpGAPDH binding was arbitrarily adjusted to 100%, and the BSA and peptide values were normalized accordingly. Data obtained in four independent experiments are shown.

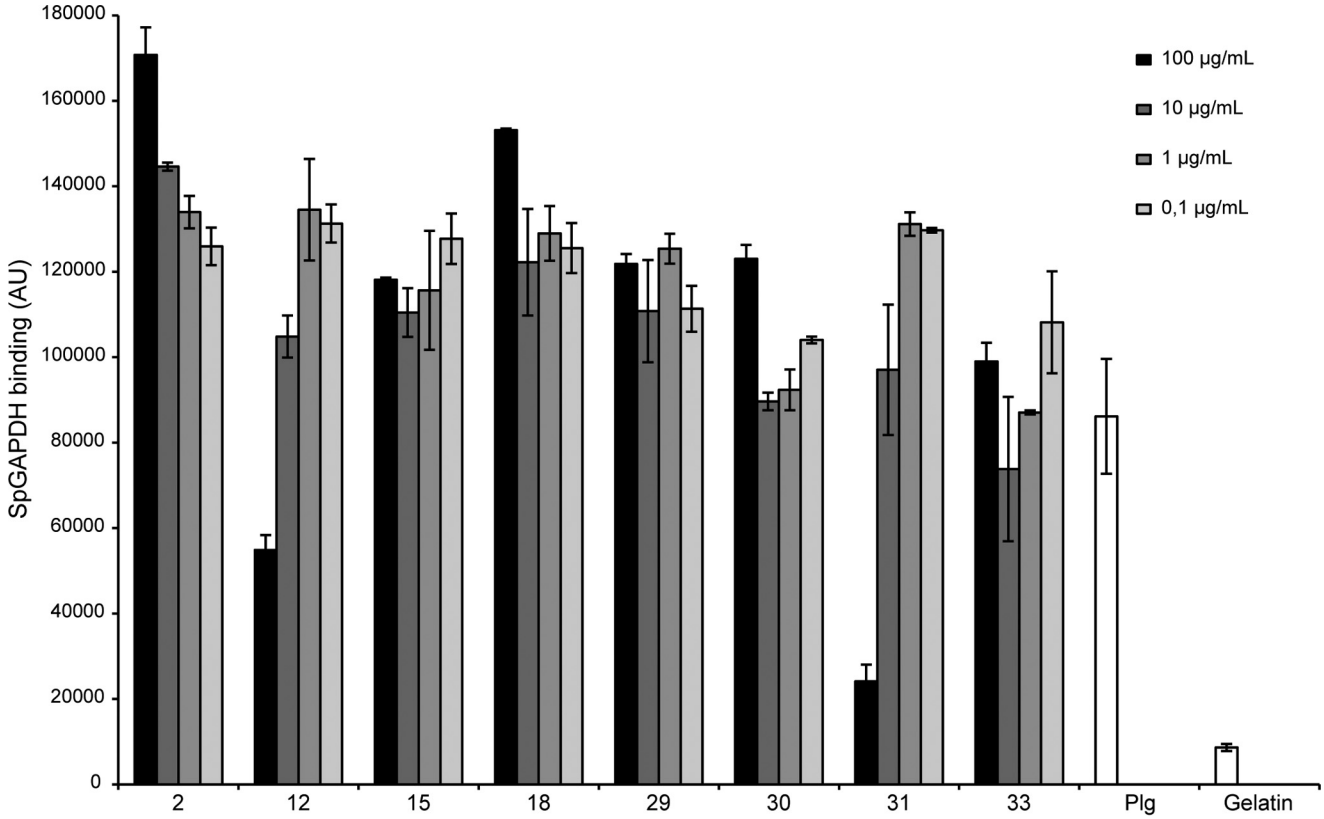


FIGURE 3. **Peptide competition for SpGAPDH association to Plg.** Plg (1 $\mu$g) was deposited on 96-well plates in duplicate and incubated with SpGAPDH peptides p2, p12, p15, p18, p29, p30, p31, and p33 at various concentrations (0.1–100 $\mu$g/ml). A solution of 2% gelatin was coated as negative control. After extensive washes, SpGAPDH (14 $\mu$g/well) was added to each well, and binding was detected with an anti-SpGAPDH antibody. In wells coated with Plg and gelatin (denoted by *Plg* and *Gelatin*), no peptide was added, represented by *white bars*. These wells are considered as positive and negative controls for SpGAPDH binding. *Error bars* represent standard deviation of duplicates. *AU*, arbitrary units.

**TABLE 2**

**Data collection and structure refinement statistics**

a.u., asymmetric unit.

| | |
|---|---|
| **Data collection statistics** | |
| Space group | C2 |
| Unit cell lengths (Å) | 80.04, 130.22, 79.84 |
| Unit cell angles (°) | 90, 119.63, 90 |
| Resolution (Å)[a] | 50.0–2.00 (2.12–2.00) |
| Monomers/a.u. | 2 |
| $R_{sym}$[a] | 5.3 (50.4) |
| % completeness[a] | 99.6 (99.5) |
| $I/\sigma(I)$ average[a] | 15.8 (2.9) |
| No. of observed reflections[a] | 186,532 (29,648) |
| No. of unique reflections[a] | 48531 (7816) |
| $CC_{½}$[a] | 99.9 (92.1) |
| Mean Wilson B | 39.7 |
| **Model refinement statistics** | |
| $R_{work}$ | 0.1953 |
| $R_{free}$ | 0.2148 |
| Root mean square deviation bonds (Å) | 0.005 |
| Root mean square deviation angles (°) | 0.880 |

[a] Values in parentheses represent the highest resolution shell.

**TABLE 3**

**Structural comparison of SpGAPDH with GAPDH from other species**

RMSD, root mean square deviation bonds; Seq. id., sequence identity.

| Species | RMSD | Seq. id. | Number aligned | PDB code |
|---|---|---|---|---|
| | *Å* | % | | |
| *Kluyveromyces marxianus* | 1.40 | 46.0 | 302 | 2I5P |
| *Bacillus anthracis* | 1.35 | 46.5 | 314 | 4DIB |
| *Homo sapiens* | 1.38 | 47.7 | 325 | 4WNC |
| *Alcaligenes xylosoxidans* | 1.13 | 50 | 325 | 1OBF |
| *Staphylococcus aureus* | 1.02 | 69.0 | 336 | 3LVF |
| *Staphylococcus aureus* | 1.13 | 69.4 | 336 | 3VAZ |
| *Streptococcus agalactiae* | 1.03 | 91.5 | 331 | 4QX6 |

of the C2 space group two-fold symmetry. The overall fold of each SpGAPDH monomer is very similar to the GAPDH structures determined so far, as expected from the high sequence identity level and conserved fold. The highest structural and sequence similarity is found with the *Streptococcus agalactiae* GAPDH structure (Table 3). We showed that lysine residues contribute to SpGAPDH-Plg interaction and that p12 and p31 contain the binding site determinants. We thus looked for surface-exposed lysines in p12 and p31 peptide sequences and observed that $Lys^{115}$ and $Lys^{304}$ are fully exposed (Fig. 4). Plg-binding sites are often composed by sequentially and/or structurally aligned lysine residues (9). Interestingly, $Lys^{116}$ is partially exposed and contiguous to $Lys^{115}$, and $Lys^{304}$ is located at the dimer interface, which results in a face-to-face positioning (Fig. 4*A*). The residues $Lys^{115}$, $Lys^{116}$, and $Lys^{304}$ were thus considered as serious candidates for defining the Plg-binding site of SpGAPDH.

The C-terminal sequence of SpGAPDH, $^{332}$KIAK$^{335}$, has been suggested to be part of the Plg-binding site (18). Our data do not directly support this observation because p33 neither displayed significant binding property to Plg nor inhibited Plg association with SpGAPDH. Furthermore, the X-ray structure shows that $Lys^{332}$ and $Lys^{335}$ are not in a favorable configuration to interact with Plg because they are partially buried (Fig. 4*B*). It is compelling to note that $Lys^{304}$ is found in a loop extension (between $\beta$16 and $\beta$17 strands),

absent in human GAPDH but present in the crystal structures of GAPDH from *Staphylococcus aureus* (3LVF) and *S agalactiae* (4QX6) (Fig. 5) (19).

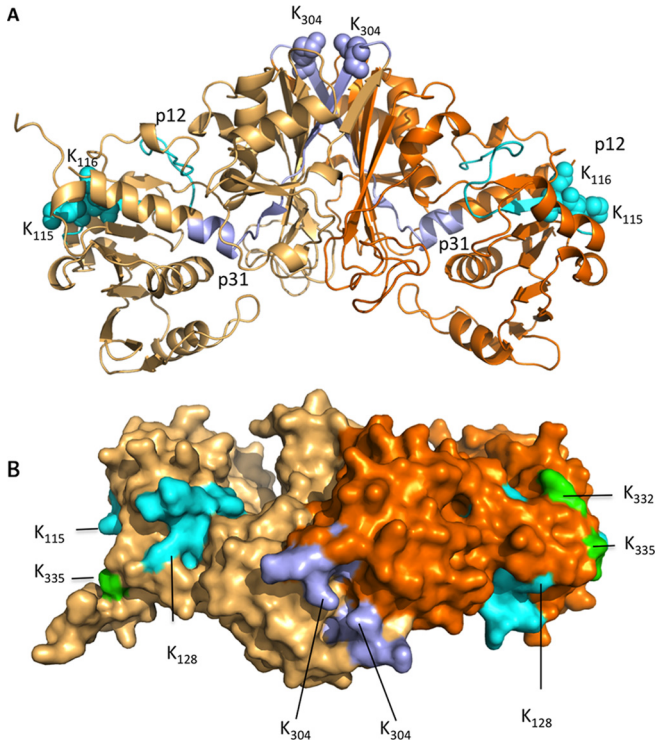


FIGURE 4. **Crystal structure of SpGAPDH and location of lysine residues involved in Plg binding.** *A*, SpGAPDH dimer is represented (PDB: 5M6D). Each monomer is colored in *light* and *dark orange*. The sequence corresponding to p12 and p31 is highlighted in *cyan* and *purple*, respectively, in both molecules. The lysine residues present in p12 and p31, and solvent-exposed residues are represented as *spheres*. $Lys^{304}$ in p31 is positioned at the dimer interface, resulting in a face-to-face configuration. $Lys^{115}$-$Lys^{116}$ in p12 form a pair of lysines partially exposed at the molecular surface. *B*, surface exposure of SpGAPDH lysines. In p12 and p31 (same color code as in *A*), $Lys^{304}$ and $Lys^{115}$ protrude out of the surface. The C-terminal lysines $Lys^{332}$ and $Lys^{335}$ (*green*) are partially exposed, as is $Lys^{128}$.

*SPR Analyses of the Plasminogen Binding Capacity of SpGAPDH Mutants*—The potential role of Plg in binding of residues $Lys^{115}$, $Lys^{116}$, and $Lys^{304}$ was investigated. The interaction of wild-type SpGAPDH, single K304A, double K115S/K116S, and triple K115S/K116S/K304A mutants with immobilized Plg was analyzed by SPR using single cycle kinetics experiments (Fig. 6). Although the K115S/K116S mutant retained its capacity to interact with immobilized plasminogen, the interaction of the K304A mutant was strongly reduced and the combination of the mutations almost abolished the interaction. Fitting of the binding data for wild-type SpGAPDH to a simple 1:1 model yielded association and dissociation rate constants of $4.74\ 10^4\ M^{-1}\ s^{-1}$ and $8.19\ 10^{-5}\ s^{-1}$, respectively, and a resulting apparent equilibrium dissociation constant ($K_D = k_d/k_a$) of 1.73 nM ($\chi^2 = 2.82$), indicative of high affinity. This $K_D$ value is comparable with that determined recently for the binding of Plg to PGK ($K_D$ = 1.27 nM) (13). Analysis of the K115S/K116S mutant using the same model yielded $k_a$ and $k_d$ rate constants of $5.39\ 10^4\ M^{-1}\ s^{-1}$ and $5.85\ 10^{-4}\ s^{-1}$ and a resulting $K_D$ value of 10.8 nM. The increase in $K_D$ resulted mainly from a 7-fold increase in $k_d$, reflecting a decreased stability of the complex. In addition, the mutant binding data were best fitted with the "two-state" interaction model, involving conformational changes of the proteins during the binding event ($\chi^2$ of 1.81 instead of 14.9 using the 1:1 model). However, the resulting apparent affinity constant ($K_D$) obtained with this model was 8.86 nM, a value close to that obtained with the 1:1 model. These results indicate that the K304A mutation prevents the interaction, whereas the K115S/K116S mutation has a negative impact on the stability of the complex.

## Discussion

Recruitment of host Plg by pathogens is emerging as a central process in virulence. Indeed, major bacterial pathogens and fungi display Plg receptors at their cell surface and exploit the host Plg system for effective invasion and dissemination. Bacterial Plg receptors are proteins either anchored to the cell wall

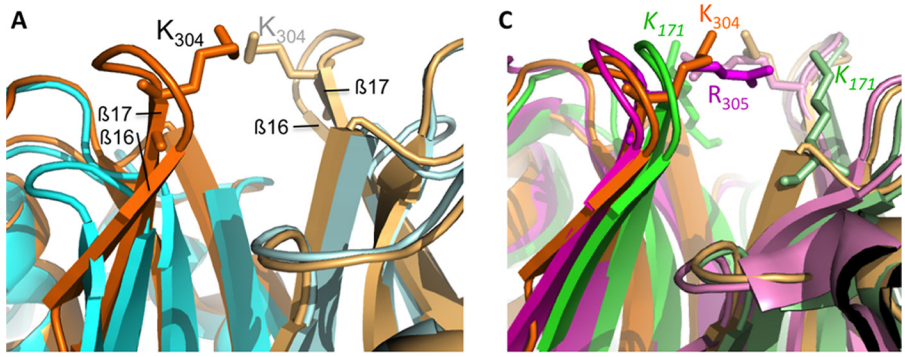


FIGURE 5. **Focus on the β16-β17 loop insertion.** *A*, this loop insertion is absent in mammal GAPDHs, as illustrated here with the structure of human GAPDH (4WNC, *cyan*/*pale cyan*) superimposed to SpGAPDH (*orange*/*pale orange*). *B*, local sequence alignment of the β16/β17 region: *S. pneumoniae* (*Spn*), *S. agalactiae* (*Sag*), and *S. aureus* (*Sau*) sequences contain the insertion, whereas it is absent in the human sequence (*Hsa*). *C*, superposition of the loop extensions in *S. agalactiae* (4QX6, green), *S. aureus* (3VAZ, *magenta*), and *S. pneumoniae* (*orange*) GAPDHs. Arginine and lysine residues exposed in the β16/β17 extension potentially part of the Plg-binding site are shown by stick representation. SauGAPDH $Arg^{305}$ is homologous to the SpGAPDH $Lys^{304}$. The lysine $Lys^{171}$ in SagGAPDH, present in a different surface loop, is located close to the two-fold axis and could also be involved in Plg binding.

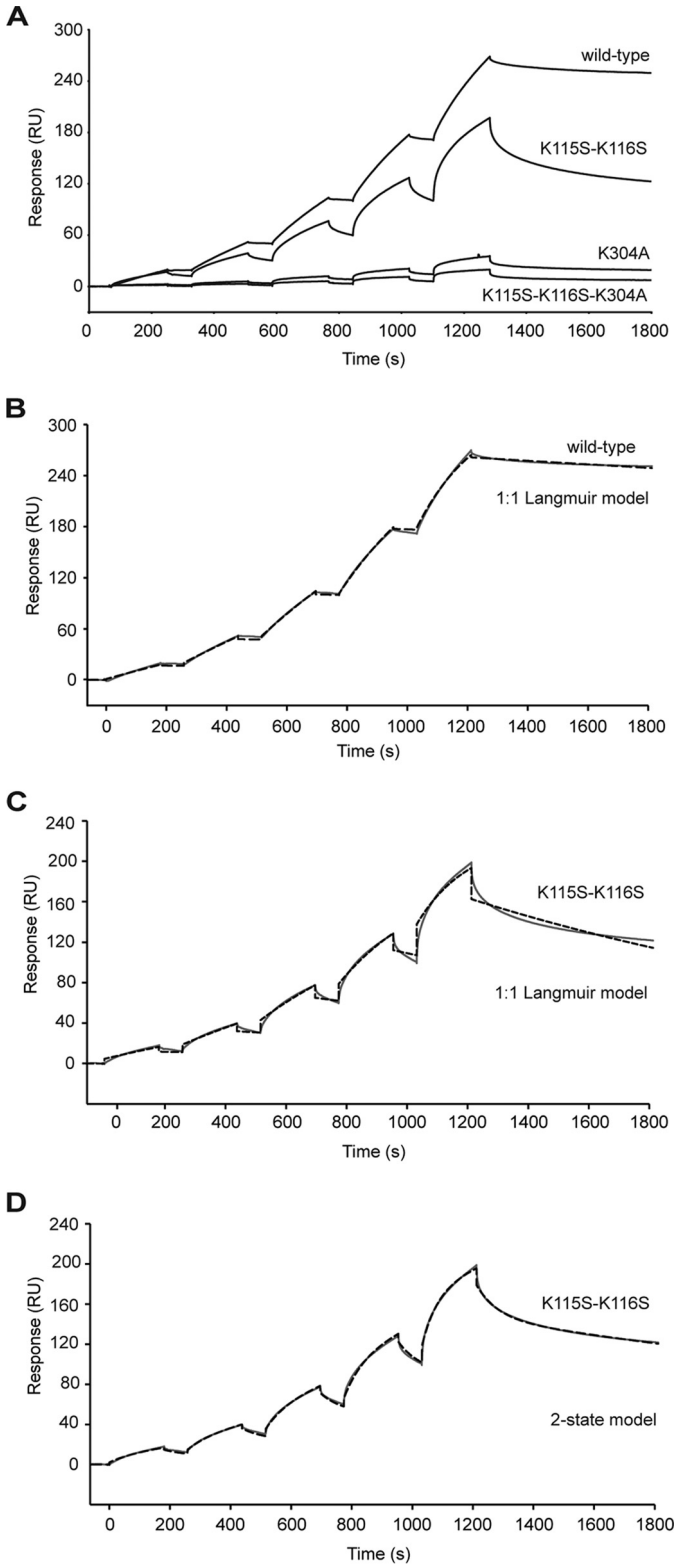


FIGURE 6. **Interaction of SpGAPDH variants with immobilized Plg.** *A*, the binding curves were obtained in single cycle mode by injecting increasing concentrations of SpGAPDH (6.25, 12.5, 25, 50, and 100 nM) at a flow rate of 30 $\mu$l/min for 180 s on immobilized Plg (2625 RU). *B–D*, kinetic analyses of binding of wild-type GAPDH (*B*) and the K115S/K116S mutant (*C* and *D*). Fits are shown as *dotted lines* and were obtained by global fitting of the data using a 1:1 Langmuir binding model (*B* and *C*) or a two-state reaction (conformational change) model (*D*). These results are representative of two independent experiments.

or related to the moonlighting class. A review published in 2012 (20) provides an overview of known bacterial Plg receptors, as well as their binding characteristics, mechanisms of Plg recruitment, and role in bacteria-host interactions. *S. pneumoniae*, similarly to other bacterial species, has evolved multiple Plg receptors at the cell surface. Although roles in cell adhesion, tissue invasion, and immune system evasion have been described for Plg receptors individually, the multifaceted function of Plg recruitment and the relevance of each Plg receptor in the virulence process of the pneumococcus still remain to be deciphered.

Cell wall-anchored proteins such as CbpE, PavB, and PfbA, as well as moonlighting proteins such as enolase, GAPDH, PGK, and PepO, are the Plg receptors so far identified in *S. pneumoniae* (9–11, 13–16). For some of the pneumococcal Plg receptors, the binding affinity has been determined, and all display high affinity range. As stated above, similar $K_D$ values have been measured for SpGAPDH and PGK: 1.73 and 1.27 nM, respectively (this work and Ref. 13). PepO and CBPE also display nM affinity binding to Plg (9, 14).

The location of the Plg-binding site has been determined in a few cases. In pneumococcal enolase, two adjacent C-terminal lysine residues ($Lys^{433}$-$Lys^{434}$) were first identified as Plg-binding sites (21). However, as they are buried in the crystal structure, a second motif exposed on the octamer surface and containing two lysines, $Lys^{251}$ and $Lys^{254}$, was proposed to be the primary binding site for Plg located on Kringle domains K1–3 (21, 22). In a previous study, we showed that the phosphorylcholine esterase (Pce) domain of CBPE interacts with the same K1–3 domains through lysine residues. Solving the crystal structure of the Pce domain along with site-directed mutagenesis allowed the identification of the Plg-binding region composed by lysine residues that map in a linear fashion on the surface of the Pce domain (9). Peptide-spot array combined with the crystal structure of PGK showed that the lysines involved in the binding of Plg K1–4 domains are located in the N-terminal region of PGK (13).

In this study, we have investigated the Plg-binding site on SpGAPDH by different experimental approaches. We showed that ACA, a molecule analog to lysine, completely inhibited the SpGAPDH interaction with Plg, indicating that lysine residues are major players in Plg binding. The peptide-spot array technique was used in two complementary approaches. First, binding of Plg was tested on immobilized peptides. and secondly, peptides were used in a binding competition assay.

Stringent conditions were defined to screen peptides that would bind to Plg: values should be 30% greater than the one observed with SpGAPDH in at least two independent experiments and five times the one of BSA. If these cutoff levels would have been strictly respected, only p12 and p31 should have been selected and further tested. However, to evaluate the reliability of the competition test, peptides detected in only one experiment have been integrated (p15, p18, p29, and p30). p2 and p33 were also tested: p2 was detected in two experiments, and p33 contains the C-terminal residues potentially involved in the interaction with Plg (18). The data presented in Fig. 3 confirm the peptide mapping screen and the relevance of the cutoff level because p12 and p31, the only two positive

peptides sorted out from the initial screen, inhibit the interaction. However, how these putative Plg-binding sites would be accessible at the surface of the SpGAPDH tertiary structure was a critical point to assess. To address this issue, we solved the crystal structure of SpGAPDH to map the p12 and p31 sequences. The resolution of the SpGAPDH crystal structure revealed that $Lys^{115}$-$Lys^{116}$ are surface-exposed and that the lysine residues $Lys^{304}$ from each monomer are positioned face-to-face. Mutagenesis of these residues revealed that $Lys^{304}$ is a key residue in the SpGAPDH Plg-binding site.

$Lys^{304}$ is present in the loop inserted between the $\beta16/\beta17$ strands, a hallmark of GAPDH from streptococcal, staphylococcal, and enterococcal species as well as *Listeria*, *Clostridium*, *Chlamydia*, and *Mycoplasma* (supplemental Table S1). The list of GAPDH sequences including a loop extension similar to SpGAPDH can be selectively collected using the sequence consensus motif: T(K/R)V*XX*V*XXX*QLVK*XXX*W (supplemental Table S1). At the same position as $Lys^{304}$ in SpGAPDH, arginine residues are also observed in GAPDH from other bacterial species such as $Arg^{305}$ in *S. aureus* GAPDH (Fig. 5, *A* and *B*). Although no data are available regarding the interaction of SauGAPDH with Plg, we propose that such association might be possible and that $Arg^{305}$ would be involved in the Plg-binding site. Interestingly, *S. agalactiae* GAPDH has been shown to interact with Plg (23) and contains the loop extension, although it does not contain a lysine homologous to the SpGAPDH $Lys^{304}$ position but displays $Lys^{171}$, similarly exposed at the dimer interface (Fig. 5*C*), which might be an alternative candidate residue involved in the interaction with Plg. On the contrary, HsaGAPDH does not contain such an extension between $\beta16$ and $\beta17$ strands. This feature might be correlated to the low affinity displayed by HsaGAPDH to Plg, ranging between 233 and 176 nM depending on the models (1:1 or two-state reaction) used to fit the SPR data (supplemental Fig. S1).

The experimental data obtained can be combined with the current knowledge on Plg structure/function properties (24). In their report of the X-ray crystal structure of full-length human Plg (25), the authors suggested that the molecular mechanism underlining the interaction of Plg with the bacterial receptors might influence the conformation and/or the activation of Plg, which in turn might direct the virulence process. We would thus suggest the following mode of interaction, illustrated in Fig. 7: (i) the pair of dimer $Lys^{304}$ could act as a first "anchoring" site for the interaction with Plg, probably by interacting with the K1 domain, which bears the unique accessible lysine-binding site; (ii) the second pair of lysines ($Lys^{115}$-$Lys^{116}$) would then serve to stabilize the interaction by extending it to another Kringle domain, most likely K3, which is favorably positioned in the closed and inactive conformation of plasminogen (25). We have verified that SpGAPDH-Plg bound is activable into plasmin *in vitro*; we could then propose that the position of the flexible K3 would rearrange during this second step in a position compatible with Plg activation. Although highly challenging, resolving structures of Plg complexed with receptors would be an invaluable clue to address this important question in the context of host-pathogen interaction.

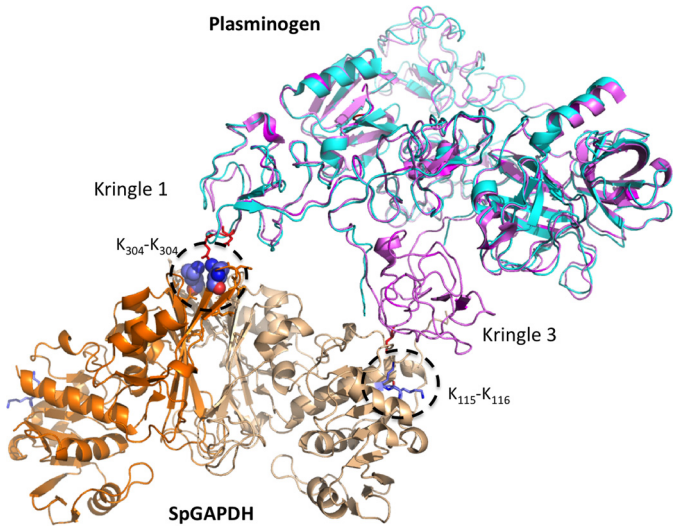


FIGURE 7. **Model of Plg/GAPDH association.** As mentioned under "Discussion," we suggest the following mode of interaction: (*a*) the pair of $Lys^{304}$ could act as a first anchoring site for the interaction with Plg, probably by interacting with the K1 domain, which bears the unique accessible lysine-binding site; (*b*) the second pair of lysines ($Lys^{115}$-$Lys^{116}$) would serve to stabilize the interaction by extending it to another Kringle domain, most likely K3. K3 is seen here in the closed conformation (4A5T, *magenta*) (32) that blocks Plg activation. Its position is appropriate to interact with the second pair of lysines, in terms of distance, but needs a reorientation to avoid steric clashes. We thus propose a reorientation of the flexible K3 (4DUU, *cyan*) (25) toward a position compatible with Plg activation during this second binding step.

## Experimental Procedures

*Cloning and Site-directed Mutagenesis*—Genomic DNA from the D39 strain of *S. pneumoniae* was used as a template to amplify the *gapdh* gene (Sp2012) by conventional PCR methodology. The full-length *gapdh* was cloned in a pQE-derived plasmid, and the resulting construct encodes the GAPDH protein fused to a $His_6$ tag at the N-terminal end. A tobacco etch virus protease cleavage site was inserted between the $His_6$ tag and the N-terminal sequence of GAPDH. HsaGAPDH fused to a $His_6$ tag at the N terminus was also expressed (17). Mutations were introduced by PCR-based site-directed mutapgenesis (QuikChange II XL Site-Directed Mutagenesis Kit, Agilent Technologies) and verified by DNA sequencing (Beckman Coulter Genomics, GENEWIZ).

*Production and Purification of SpGAPDH Variants*—Protein expression and purification protocols of native and mutant forms of SpGAPDH, as well as of HsaGAPDH, were similar. Overnight cultures of the *Escherichia coli* BL21(DE3)-CodonPlus-RIL (Stratagene) strain transformed with the GAPDH expression constructs were used for inoculation with 500 ml of Terrific Broth medium (Euromedex) supplemented with 100 $\mu$g/ml ampicillin and cultured at 37 °C for 3 h. Protein expression was induced with 1 mM isopropyl-$\beta$-D-1-thiogalactopyranoside for 16 h at 15 °C. After sonication and centrifugation of the lysate (20 min, 39,200 × *g*), recombinant GAPDH was recovered from the soluble fraction and loaded onto a 1-ml prepacked HisTrap HP column (GE Healthcare). Column equilibration buffer was 50 mM Tris-HCl, pH 8.0, 200 mM NaCl, 20 mM imidazole. After extensive washing, recombinant GAPDH was eluted with 60, 100, 300, and 500 mM imidazole steps in 50 mM Tris-HCl, pH 8.0, 200 mM NaCl buffer and subsequently

dialyzed against 10 mM HEPES, pH 7.4, 150 mM NaCl, 2 mM $CaCl_2$ before use for biological assays. The degree of protein purity was checked by Coomassie Blue staining of SDS-polyacrylamide gels. Protein concentration was determined by absorbance at 280 nm (extinction coefficient: 22,920 $M^{-1}$ $cm^{-1}$).

*SPR Studies*—Analyses were performed at 25 °C using a T200 instrument (GE Healthcare). Plg was diluted to 100 $\mu$g/ml in 10 mM sodium acetate, pH 5.0, and immobilized (2625 RU) on a CM5 (series S) sensor chip (GE Healthcare) in 10 mM HEPES, pH 7.4, 150 mM NaCl, 3 mM EDTA, 0.05% surfactant P20 (HBS-EP) using the amine coupling chemistry according to the manufacturer's instructions (GE Healthcare). The reference surface was prepared using the same procedure except that the protein solution was replaced by buffer. SpGAPDH binding was measured in 10 mM HEPES, pH 7.4, 150 mM NaCl, 2 mM $CaCl_2$, 0.05% surfactant P20 (HBS-CaP) at a flow rate of 30 $\mu$l/min. Regeneration of the surface was achieved by a 15-$\mu$l injection of 10 mM NaOH. The signals recorded on the reference flow cell were subtracted from those obtained on immobilized Plg.

For competition assays, GAPDH (100 nM) was incubated for 15 min at room temperature in the presence of various concentrations of ACA (Sigma, A2504) before injection over immobilized Plg. The signals recorded for injection of ACA alone were subtracted from the data. Kinetic titrations (single-cycle kinetics) were analyzed using the Biacore T200 Evaluation software 1.0.

*Peptide-spot Array*—A peptide mapping procedure was used to identify the Plg-binding regions of SpGAPDH. The sequence recorded in the database (UniProt accession number Q8CWN6) accounts for 359 residues, whereas the correct ORF starts at $Met^{25}$. Because the gene cloned to allow SpGAPDH expression starts at $Met^{25}$, the SpGAPDH produced contains 335 residues. The sequence corresponding to amino acids 3-335 was divided into 33 peptides (p1–p33); each peptide was 20 amino acids in length and overlapped the previous peptide by 10 amino acids (Millegen, France) (Table 1).

Peptides were immobilized to the PBS-washed nitrocellulose membrane (10 $\mu$g/spot) using the Dot Blotter apparatus (Denville Scientific). The membranes were washed for 15 min with PBS, and then incubated for 1 h with blocking buffer (PBS, 0.3% Tween 20, 5% fat-free milk). After extensive washing, the membrane was incubated with Plg (final concentration of 10 $\mu$g/ml) in 10 mM HEPES, pH 7.4, 150 mM NaCl, 2 mM $CaCl_2$, 0.2% gelatin, 0.05% Tween 20 (binding buffer) for 2 h. For a positive control, SpGAPDH was deposited on the nitrocellulose membrane (10 $\mu$g) and 10 $\mu$g of BSA were spotted as a negative control. After incubation, the membrane was washed three times with PBS, 0.3% Tween 20 and incubated for 1 h with goat anti-Plg antibody (Abcam, ab6189) diluted 1:5,000 in blocking buffer. After three washing steps with PBS, 0.3% Tween 20, the membranes were incubated with horseradish peroxidase-conjugated anti-goat antibody (Sigma) (1:10,000 dilution). After extensive washes with PBS, 0.3% Tween 20, 1 ml of ECL solution (Pierce) was added to the membrane and the chemiluminescence signal was recorded on photographic films. The intensity of each spot was then quantified using ImageJ software.

*Solid-phase Binding Assay*—A solid-phase binding assay was performed to test the inhibitory property of peptides. White 96-well microtiter plates (Greiner Bio-One) were coated with 1 $\mu$g of Plg or 2% gelatin as a control in 100 $\mu$l of 10 mM HEPES, pH 7.4, 150 mM NaCl, 2 mM $CaCl_2$ (binding buffer) at 4 °C overnight. Saturation was performed by adding 200 $\mu$l of binding buffer, 0.2% gelatin per well for 1 h at room temperature. Five washes were performed using 200 $\mu$l of binding buffer. Peptides were added to Plg at different concentrations, from 0.1 to 100 $\mu$g/ml in 100 $\mu$l of binding buffer, and incubated for 1 h at room temperature. After five washes, 100 $\mu$l of binding buffer containing 1 $\mu$g of SpGAPDH were added in each well and incubated for 1 h at room temperature. SpGAPDH was detected by successive incubations with an anti-GAPDH rabbit polyclonal antibody (1:2,000 dilution) and a horseradish peroxidase-conjugated anti-rabbit antibody (Sigma) (1:10,000 dilution). After extensive washes with binding buffer, 0.03% Tween 20, 100 $\mu$l of ECL solution (Pierce) were added to each well and chemiluminescence was measured using a multiwell luminescence reader (FLUOstar Optima; BMG Labtech).

*Crystallization, Data Collection, and Structure Determination*—SpGAPDH was concentrated to 7.5, 10, or 15 mg/ml. Standard crystallization kits have been screened through the European Molecular Biology Laboratory (EMBL) HTXlab platform at 20 °C. Several hits were reproduced manually, using the hanging drop method by mixing equal volumes (2 $\mu$l) of protein and reservoir solutions. The structure presented here was obtained using the following reservoir solution: 15% PEG 3350, 0.2 M trisodium citrate dihydrate, pH 8.8. The crystals were stabilized and cryo-protected by raising the PEG concentration to 20% and adding 20% glycerol. Diffraction data were recorded at the European Synchrotron Radiation Facility (ESRF) beamline ID23-eh1. The diffraction data collection were integrated and scaled with XDS (26).

The structure was initially solved by molecular replacement (27) using the dataset measured and SauGAPDH (PDB code 3LVF) coordinates as a starting model, because they share 70% sequence identity and 82% sequence similarity. Alternative cycles of refinement and interactive model corrections were performed using Refmac5 (28) and Coot (29), respectively. The final refinement cycles were performed using Phenix (30). Illustrations were prepared using PyMOL (31).

*Author Contributions*—C. M. and C. G. crystallized and solved the structure of SpGAPDH. R. T. conducted most of the experiments and analyzed the results. N. M. T. performed part of the SPR experiments and analyzed data. A. M. D. G. designed the research and analyzed data. N. M. T., C. G., T. V., and A. M. D. G. wrote the paper. All authors reviewed the manuscript.

*Acknowledgments—We thank Isabelle Bally and Jean-Baptiste Reiser for assistance and access to the SPR facility. We acknowledge the platforms of the Grenoble Instruct Centre (Integrated Structural Biology Grenoble (ISBG); UMS 3518 CNRS-CEA-UGA-EMBL) supported by the French Infrastructure for Integrated Structural Biology Initiative FRISBI (ANR-10-INSB-05-02) and by the Grenoble Alliance for Integrated Structural Cell Biology GRAL (ANR-10-LABX-49-01) within the Grenoble Partnership for Structural Biology (PSB). Access to the European Synchrotron Radiation Facility beamline ID23-eh1 is acknowledged.*

## References


1. Bhattacharya, S., Ploplis, V. A., and Castellino, F. J. (2012) Bacterial plasminogen receptors utilize host plasminogen system for effective invasion and dissemination. *J. Biomed. Biotechnol.* **2012,** 482096
2. Castellino, F. J., and Ploplis, V. A. (2005) Structure and function of the plasminogen/plasmin system. *Thromb. Haemost.* **93,** 647–654
3. Deryugina, E. I., and Quigley, J. P. (2012) Cell surface remodeling by plasmin: a new function for an old enzyme. *J. Biomed. Biotechnol.* **2012,** 564259
4. Syrovets, T., Lunov, O., and Simmet, T. (2012) Plasmin as a proinflammatory cell activator. *J. Leukoc. Biol.* **92,** 509–519
5. O'Brien, K. L., Wolfson, L. J., Watt, J. P., Henkle, E., Deloria-Knoll, M., McCall, N., Lee, E., Mulholland, K., Levine, O. S., Cherian, T., and Hib and Pneumococcal Global Burden of Disease Study Team (2009) Burden of disease caused by *Streptococcus pneumoniae* in children younger than 5 years: global estimates. *Lancet* **374,** 893–902
6. Bergmann, S., Schoenen, H., and Hammerschmidt, S. (2013) The interaction between bacterial enolase and plasminogen promotes adherence of *Streptococcus pneumoniae* to epithelial and endothelial cells. *Int. J. Med. Microbiol. IJMM* **303,** 452–462
7. Attali, C., Durmort, C., Vernet, T., and Di Guilmi, A. M. (2008) The interaction of *Streptococcus pneumoniae* with plasmin mediates transmigration across endothelial and epithelial monolayers by intercellular junction cleavage. *Infect. Immun.* **76,** 5350–5356
8. Frolet, C., Beniazza, M., Roux, L., Gallet, B., Noirclerc-Savoye, M., Vernet, T., and Di Guilmi, A. M. (2010) New adhesin functions of surface-exposed pneumococcal proteins. *BMC Microbiol.* **10,** 190
9. Attali, C., Frolet, C., Durmort, C., Offant, J., Vernet, T., and Di Guilmi, A. M. (2008) *Streptococcus pneumoniae* choline-binding protein E interaction with plasminogen/plasmin stimulates migration across the extracellular matrix. *Infect. Immun.* **76,** 466–476
10. Jensch, I., Gámez, G., Rothe, M., Ebert, S., Fulde, M., Somplatzki, D., Bergmann, S., Petruschka, L., Rohde, M., Nau, R., and Hammerschmidt, S. (2010) PavB is a surface-exposed adhesin of *Streptococcus pneumoniae* contributing to nasopharyngeal colonization and airways infections. *Mol. Microbiol.* **77,** 22–43
11. Yamaguchi, M., Terao, Y., Mori, Y., Hamada, S., and Kawabata, S. (2008) PfbA, a novel plasmin- and fibronectin-binding protein of *Streptococcus pneumoniae*, contributes to fibronectin-dependent adhesion and antiphagocytosis. *J. Biol. Chem.* **283,** 36272–36279
12. Henderson, B., and Martin, A. (2011) Bacterial virulence in the moonlight: multitasking bacterial moonlighting proteins are virulence determinants in infectious disease. *Infect. Immun.* **79,** 3476–3491
13. Fulde, M., Bernardo-García, N., Rohde, M., Nachtigall, N., Frank, R., Preissner, K. T., Klett, J., Morreale, A., Chhatwal, G. S., Hermoso, J. A., and Bergmann, S. (2014) Pneumococcal phosphoglycerate kinase interacts with plasminogen and its tissue activator. *Thromb. Haemost.* **111,** 401–416
14. Agarwal, V., Kuchipudi, A., Fulde, M., Riesbeck, K., Bergmann, S., and Blom, A. M. (2013) *Streptococcus pneumoniae* endopeptidase O (PepO) is a multifunctional plasminogen- and fibronectin-binding protein, facilitating evasion of innate immunity and invasion of host cells. *J. Biol. Chem.* **288,** 6849–6863
15. Bergmann, S., Rohde, M., Chhatwal, G. S., and Hammerschmidt, S. (2001) α-Enolase of *Streptococcus pneumoniae* is a plasmin(ogen)-binding protein displayed on the bacterial cell surface. *Mol. Microbiol.* **40,** 1273–1287
16. Bergmann, S., Rohde, M., and Hammerschmidt, S. (2004) Glyceraldehyde-3-phosphate dehydrogenase of *Streptococcus pneumoniae* is a surface-displayed plasminogen-binding protein. *Infect. Immun.* **72,** 2416–2419
17. Terrasse, R., Tacnet-Delorme, P., Moriscot, C., Pérard, J., Schoehn, G., Vernet, T., Thielens, N. M., Di Guilmi, A. M., and Frachet, P. (2012) Human and pneumococcal cell surface glyceraldehyde-3-phosphate dehydrogenase (GAPDH) proteins are both ligands of human C1q protein. *J. Biol. Chem.* **287,** 42620–42633
18. Bergmann, S., and Hammerschmidt, S. (2007) Fibrinolysis and host response in bacterial infections. *Thromb. Haemost.* **98,** 512–520
19. Ayres, C. A., Schormann, N., Senkovich, O., Fry, A., Banerjee, S., Ulett, G. C., and Chattopadhyay, D. (2014) Structure of *Streptococcus agalactiae* glyceraldehyde-3-phosphate dehydrogenase holoenzyme reveals a novel surface. *Acta Crystallogr. F Struct. Biol. Commun.* **70,** 1333–1339
20. Sanderson-Smith, M. L., De Oliveira, D. M. P., Ranson, M., and McArthur, J. D. (2012) Bacterial plasminogen receptors: mediators of a multifaceted relationship. *J. Biomed. Biotechnol.* **2012,** 272148
21. Bergmann, S., Wild, D., Diekmann, O., Frank, R., Bracht, D., Chhatwal, G. S., and Hammerschmidt, S. (2003) Identification of a novel plasmin (ogen)-binding motif in surface displayed α-enolase of *Streptococcus pneumoniae*. *Mol. Microbiol.* **49,** 411–423
22. Ehinger, S., Schubert, W.-D., Bergmann, S., Hammerschmidt, S., and Heinz, D. W. (2004) Plasmin(ogen)-binding α-enolase from *Streptococcus pneumoniae*: crystal structure and evaluation of plasmin(ogen)-binding sites. *J. Mol. Biol.* **343,** 997–1005
23. Seifert, K. N., McArthur, W. P., Bleiweis, A. S., and Brady, L. J. (2003) Characterization of group B streptococcal glyceraldehyde-3-phosphate dehydrogenase: surface localization, enzymatic activity, and protein-protein interactions. *Can. J. Microbiol.* **49,** 350–356
24. Law, R. H. P., Abu-Ssaydeh, D., and Whisstock, J. C. (2013) New insights into the structure and function of the plasminogen/plasmin system. *Curr. Opin. Struct. Biol.* **23,** 836–841
25. Law, R. H. P., Caradoc-Davies, T., Cowieson, N., Horvath, A. J., Quek, A. J., Encarnacao, J. A., Steer, D., Cowan, A., Zhang, Q., Lu, B. G. C., Pike, R. N., Smith, A. I., Coughlin, P. B., and Whisstock, J. C. (2012) The X-ray crystal structure of full-length human plasminogen. *Cell Rep.* **1,** 185–190
26. Kabsch, W. (2010) XDS. *Acta Crystallogr. D. Biol. Crystallogr.* **66,** 125–132
27. McCoy, A. J., Grosse-Kunstleve, R. W., Adams, P. D., Winn, M. D., Storoni, L. C., and Read, R. J. (2007) Phaser crystallographic software. *J. Appl. Crystallogr.* **40,** 658–674
28. Murshudov, G. N., Skubák, P., Lebedev, A. A., Pannu, N. S., Steiner, R. A., Nicholls, R. A., Winn, M. D., Long, F., and Vagin, A. A. (2011) REFMAC5 for the refinement of macromolecular crystal structures. *Acta Crystallogr. D. Biol. Crystallogr.* **67,** 355–367
29. Emsley, P., Lohkamp, B., Scott, W. G., and Cowtan, K. (2010) Features and development of Coot. *Acta Crystallogr. D. Biol. Crystallogr.* **66,** 486–501
30. Adams, P. D., Afonine, P. V., Bunkóczi, G., Chen, V. B., Davis, I. W., Echols, N., Headd, J. J., Hung, L.-W., Kapral, G. J., Grosse-Kunstleve, R. W., McCoy, A. J., Moriarty, N. W., Oeffner, R., Read, R. J., Richardson, D. C., *et al.* (2010) PHENIX: a comprehensive Python-based system for macromolecular structure solution. *Acta Crystallogr. D. Biol. Crystallogr.* **66,** 213–221
31. DeLano, W. L. (2012) *The PyMOL Molecular Graphics System*, version 1.5.0.1, Schrödinger, LLC, New York
32. Xue, Y., Bodin, C., and Olsson, K. (2012) Crystal struture of the native plasminogen reveals an activation-resistant compact conformation. *J. Thromb. Haemost.* **10,** 1385–1396